Macromolecules

ARTICLE

pubs.acs.org/Macromolecules

A Particle Tracking Velocimetric Study of Interfacial Slip at Polymer−Polymer Interfaces

Gregory D. Zartman and Shi-Qing Wang*

Department of Polymer Science, University of Akron, Akron, Ohio 44325-3909, United States

ABSTRACT:

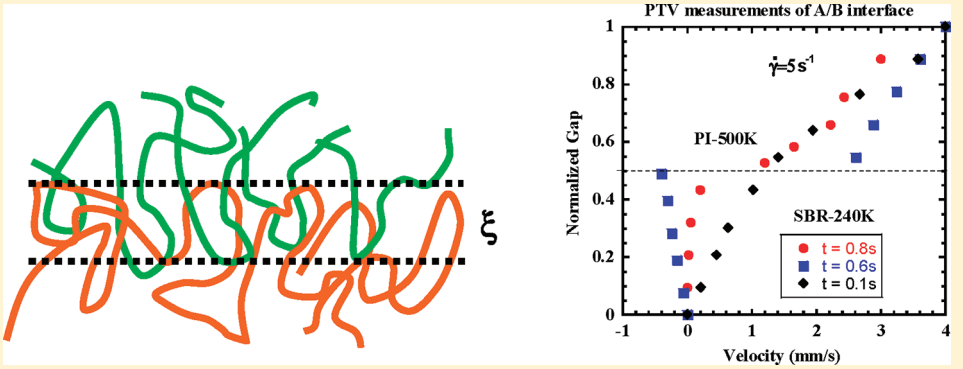

Particle tracking velocimetry (PTV) was used in conjunction with rheological measurements to investigate slip at polymer−polymer interfaces during and after startup shear using simple shear geometry, i.e., a sliding plate rheometer. Polymer pairs include styrene butadiene rubber (SBR) and polyisoprene (PI) of narrow molecular weight distribution, as well as a PI and polydimethylsiloxane (PDMS), with Flory interaction parameter $\chi \approx 0.001$ and $\chi \approx 0.08$ respectively. During startup shear, the SBR-PI pair was able to deform without interfacial failure up to a critical strain $\gamma = 2$, revealing a level of interfacial strength consistent with thermodynamic considerations. This pair also exhibited arrested interfacial slip after shear cessation for high Weissenberg numbers when the step strain exceeds unity. In contrast, the PDMS−PI interface is much weaker, and slip occurs at γ as low as 0.1. These results shed light on the nature of possible mechanical failure at interphases in multicomponent polymer systems during shear and after shear cessation.

I. INTRODUCTION

Almost all polymer products are blends or are made of a variety of different polymers with immiscible polymer interfaces. Despite the prevalence of theses interfaces, no study has addressed their startup shear behavior, which is among the most important component of polymer compounding and processing.

Slip at polymer-solid interfaces has been well studied, and many phenomena including stick−slip have been delineated.[1−4] On the other hand, polymer−polymer interfacial slip is less well studied and understood. The first clue of polymer−polymer slip came when researchers found negative deviations from various empirical viscosity mixture rules, with viscosities sometimes lower than either component.[5−7] These abnormally low viscosities were first credited to slip between difference phases by Lin and subsequently by other workers.[5,7,8]

It is known that slip can play a role in the toughness of multiphase solids and in adhesion between multiple layers.[9] Polymer−polymer slip is also the driving force behind processing additives that allow slip to occur so as to avoid flow complications such as sharkskin and die swell.[10] The same study by Migler et al. used a less sophisticated version of particle tracking and found large slip velocities on the order 10 mm/s for a fluoropolymer and linear low-density polyethylene.[10]

The first studies of polymer interfaces, where both polymers are in their liquid states, appear to be those of Lee et al.[11] and Zhao et al.[12] who inferred interfacial slip indirectly using multiple layers. These studies involve characterization of interfacial slip only in steady state shear flow. Theoretical and computational accounts of polymer−polymer interfaces can often explain equilibrium and steady flow cases.[13,14] The present study examines the transient response of such interfaces using particle-tracking velocimetry (PTV) and a sliding plate rheometer. The objective is to learn about how strong a given polymer−polymer interface is and when interfacial slip occurs upon a startup shear. In particular, the PTV directly visualizes the interfacial failure and estimates the slip velocity V_s at PI−SBR and PI−PDMS interfaces respectively at room temperature, where all of these polymers are melts.

II. THEORETICAL BACKGROUND

In order to understand how slip occurs at incompatible polymer interfaces it is helpful to picture an interface with

Received: August 23, 2011
Revised: October 25, 2011
Published: November 28, 2011

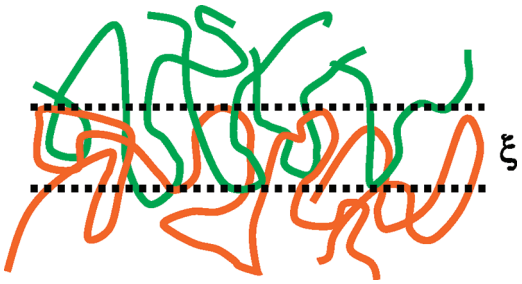

Figure 1. Chain level depiction of a typical incompatible polymer−polymer interface.

incompatible polymers on each side as shown in Figure 1. Such an interface can be prepared between polymer A and polymer B by placing them in contact with each other. The interface starts out very sharp with little or no molecular interdigitation. Over time chains protrude into the opposite side of the interface with an enthalpic cost for m monomers:

$$\Delta H_m \sim m\chi k_B T \tag{1}$$

where χ is the Flory chi parameter,[15] k_B the Boltzmann constant, and T the absolute temperature. Assuming that ΔH_m is on the order of $k_B T$, we have an average value of m equal to $\overline{m} \sim 1/\chi$. If the blob in the interface is Gaussian with a coil size ξ, the interfacial thickness is then given by

$$\xi = a\sqrt{\overline{m}} = \frac{a}{\sqrt{\chi}} \tag{2}$$

where a is a statistical segment length. This estimate based on scaling actually agrees with a more rigorous calculation: Helfand and Tagami applied a rigorous self-consistent field calculation for a flat polymer interface and found an expression for the thickness of an interfacial region ξ in terms of the Flory parameter χ and a, assuming an infinite degree of polymerization.[16]

$$\xi = \frac{2a}{\sqrt{6\chi}} \tag{3}$$

In terms of ξ, the shear stress at the interface during slip can be calculated by the following expression:

$$\sigma = \frac{\eta_i V_s}{\xi} \tag{4}$$

where the slip velocity V_s is depicted in Figure 2, and η_i is the viscosity at the interface.

Past studies of slip at polymer/solid interfaces[17] and between polymers[18] have used an extrapolation length b defined as:

$$b = \frac{V_s}{\dot{\gamma}} = \frac{\eta}{\eta_i}\xi \tag{5}$$

in terms of the slip velocity V_s, local shear rate $\dot{\gamma}$, the bulk viscosity η, and the viscosity η_i in the slip layer of thickness ξ. This definition works well when measuring the slip of single component systems against solid walls. For slip at polymer−polymer interface we propose to use a dimensionless number V_s/V_a to characterize the degree of interfacial slip, where V_a is the applied velocity. The magnitude of the slip velocity V_s relative to V_a can be written in terms of the slip length b_1 and b_2 with respective to the two media as

$$\frac{V_s}{V_a} = \frac{b_1/H_1}{1 + b_1/H_1 + (H_2/H_1)\dfrac{b_1}{b_2}} \tag{6}$$

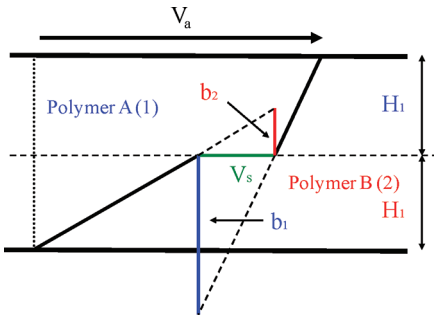

Figure 2. Illustration of interfacial slip with slip velocity V_s, where an extrapolation length b can be defined relative to each of the two polymers.

where H_1 and H_2 are the thickness of the individual components. This measure of slip provides a number between 0 and 1, with 1 being complete slip and 0 representing negligible slip. It is a unique combination of the two slip lengths that quantifies how much of the applied velocity is accounted for by the interfacial slip.

III. EXPERIMENTAL SECTION

A. Materials. This study focuses primarily on the interfaces made of highly entangled polymer melts, namely, a linear styrene butadiene rubber (SBR) with 21% styrene and 79% 1,4-butadiene, received from Xiaorong Wang of Bridgestone, two relatively monodisperse polyisoprene (PI) melts (labeled as PI300 K and PI500 K) courtesy of Dr. Adel Halasa at Goodyear, with similar microstructures: *cis*-1,4 (75.2%), *trans*-1,4 (17.8%), and −3.4 (7.0%) for PI300 K and *cis*-1,4 (75.0%), *trans*-1,4 (16.4%), and −3.4 (6.6%) for PI550 K, and a commercial polydimethylsiloxane (PDMS) from GE Silicones (product number: SE54). Table 1 contains the molecular characteristics of the materials from small amplitude oscillatory shear measurements of their storage and loss moduli as a function of frequency that were carried out with an Anton Paar Physica MCR 301 rheometer. Parts a−d of Figures 3 respectively show the storage and loss moduli G' and G'' of these polymer melts. Molecular weight and PDI where found using GPC, SEC was done using a Wyatt Dawn Eos multiangle laser light (MALLS) detector plus waters model 2414 differential refractometer concentration detector. This was coupled with Wyatt Astra V 4.73.04 software and 3 waters HR styrogel columns using THF at 35 °C flowing at 1 mL/min. Table 1 also lists the literature values[19] of polymer entanglement spacing l_{ent} for all the melts under study. Table 2 contains the values of the statistical segment length a, which were calculated as follows. Helfand and Tagami defined the segment length a as:

$$\langle R^2 \rangle = Na^2 \tag{7}$$

where $\langle R^2 \rangle$ is the average end-to-end distance squared and N is the degree of polymerization. In terms of the characteristic ratio C_∞ and backbone length l we have

$$\langle R^2 \rangle = C_\infty n l^2 = Na^2 \quad \text{and} \quad a = \sqrt{\frac{nC_\infty}{N}}l \tag{8}$$

where n is the number of backbone bonds. To find the value for a of a given polymer pairs, a geometric average was used,[14] i.e., $a = (a_1 a_2)^{1/2}$. Table 3 contains the estimated interfacial thickness ξ using eq 1 and χ values calculated based on the solubility parameters.[20,21]

In order to perform PTV observations, all the samples were impregnated with about 400 ppm silver-coated particles with an average size of 10 μm by solution mixing with toluene. The solutions with consistency of honey were then poured into a tray to allow evaporation

dx.doi.org/10.1021/ma201929q |*Macromolecules* 2011, 44, 9814–9820

Table 1. Basic Characteristics of Four Polymer Melts

sample	M_n (kg/mol)	M_w/M_n	G_N^0 (MPa)	M_e (kg/mol)	M_w/M_e	l_e (nm)	τ (s)
PI300 K	291	1.07	0.40	5.1	61	6.2	4.9
PI500 K	516	1.06	0.40	5.1	107	6.2	50.0
SBR240 K	241	1.10	0.82	2.7	98	5.1	34.0
PDMS540 K	539	1.63	NA	9.6	91	7.8	1

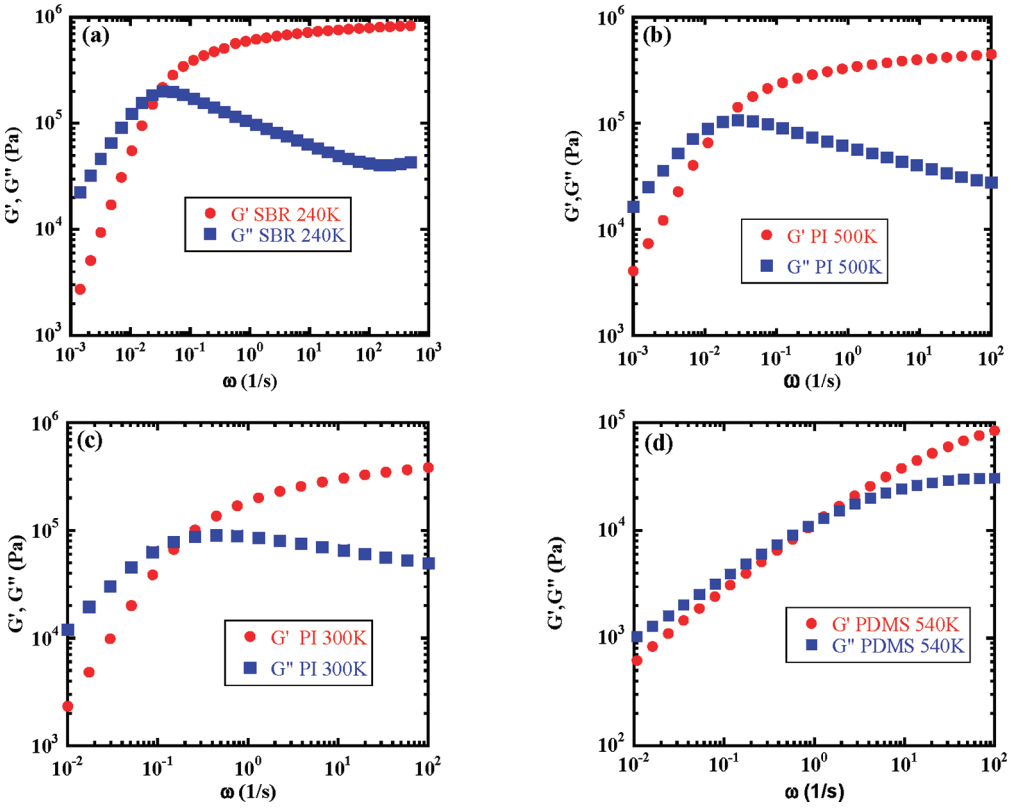

Figure 3. Small amplitude oscillatory shear (SAOS) data for (a) SBR 240 K, (b) PI 550 K, (c) PI 300 K and (d) PDMS 540 K.

of the toluene under a fume hood for 1 week, followed by a minimum of 48 h in a vacuum oven. Bubble free films (with typical thickness of ca. 0.1 mm) were stacked to make a final sample with thickness of ca. 0.4 mm using a Carver brand press. Two films with an area of 10 mm by 40 mm were then stacked and pressed under nominal normal force to remove any macroscopic bubbles at the interface and creating a sheet-like sample with a total thickness around 0.8 mm. Commercially available Krazy Glue was then used to adhere the top and bottom surfaces of the two-layered sample to the upper and lower plates of the sliding plate rheometer (SPR). This is done to prevent wall slip at the sample-plate interfaces and ensure the no-slip boundary condition. Wall slip, i.e., sample/plate slip can occur under the relevant shearing conditions because the PI-SBR interface can be as strong as the polymer/plate interface. The samples were left in equilibrium in the rheometer overnight. In our SPR, the bottom plate is fixed and upper plate is displaced by a step motor (Motion Parker Co., model ZETA6104−57−83). A load cell (Honey Well Co., model 13) was used to measure the force produced by the sample in resisting the imposed shear and during stress relaxation, along with PTV from the perspective of Figure 2. The PTV allowed viewing of the velocity profile in real time. Video recording the velocity profile as a function of time permits us to capture the exact moment and corresponding strain when any interfacial slip occurs, to measure the slip velocity, and to ensure that the experiment was free of wall slip and other instabilities. More details about both PTV and the custom-made sliding plate rheometer are available elsewhere.[22,23]

Table 2. Basic Chain Statistical Properties

	l (Å)	C_∞	a (Å)
PI	1.54	4.6	6.6
PDMS	1.63	6.8	6.0
PS	1.54	9.5	6.7
PBD	1.54	5.3	7.1
SBR	1.54	NA	7.0

RESULTS AND DISCUSSIONS

Startup shear mode has been performed with our sliding-plate rheometer to explore nonlinear rheological phenomena such as polymer-solid interfacial slip[24] and elastic yielding instability.[25] In the present PTV-based study, startup shear is used to probe how interfacial slip occurs between two immiscible polymers. The present study reveals polymer−polymer interfacial yielding in two different manifestations, namely, interfacial slip during shear and arrested slip after shear cessation.

Interfacial Yielding during Startup Shear. The SBR240 K/PI500 K interface fails universally during startup shear at a strain $\gamma \sim 2$ at the nominal rates (i.e., $V_a/H = \dot{\gamma}$) in the range of $1\ s^{-1} \leq \dot{\gamma} \leq 12\ s^{-1}$. On the other hand, the interfaces fail at lower stains (<2) when sheared at the lower rates such as $\dot{\gamma} = 0.05\ s^{-1}$, $\dot{\gamma} = 0.12\ s^{-1}$, and $\dot{\gamma} = 0.5\ s^{-1}$. This interfacial breakdown occurs just beyond the stress maxima recorded in Figure 4, parts a and b, and was confirmed simultaneously by PTV. Since there is significant stress buildup, comparable to the level of the melt plateau modulus of polyisoprene as shown in Figure 4b, we can infer that there must be significant mutual chain entanglement between SBR and PI. Such a conclusion is consistent with the estimated interfacial thickness ξ for SBR/PI pair, which is large enough to permit sufficient interpenetration and chain entanglement between SBR and PI. In other words, ξ is about three times as large as the entanglement spacing according to Tables 1 and 3. Consequently, the interfacial slip follows a similar yielding process as described previously for a polymer/wall interface:[22] At the stress maximum, force imbalance occurs between the growing elastic retraction force of intrachain origin and the intermolecular gripping force between polymer A and polymer B. As seen before for wall slip, we see strong recoil in Figure 4, parts c and d. Also worth noting in Figure 4c at $t = 10$ s is that V_s is even greater than the applied velocity of 0.1 mm/s during elastic recoil shortly after interfacial failure.

Table 3. Interfacial Thickness of Two Polymer Pairs

sample pair	a (Á)	χ	ξ (nm)
SBR240 K/PI500 K	6.8	0.001	18
PI300 K/PDMS540 K	6.3	0.08	1.8

These well interdigitated samples, i.e., well-healed interfaces, exhibit three stages in their response to startup shear. First, the sample undergoes elastic shear deformation without interfacial failure. This is evident for $t < 5$ s in Figure 4c and $t < 0.1$ s in Figure 4d, where t represents the time elapsed since the onset of shear. For the imposed fast shear, the initial sample response is elastic. Therefore, we can expect the velocity profile to be dictated by the transient elastic moduli of polymers A and B. In other words, the different velocity gradients in the different layers reflect the difference in the elastic stiffness of the entangled melts. Figure 5 accentuates this point by showing the velocity profile of SBR and PI at $V_a/H = \dot{\gamma} = 8.25\ s^{-1}$ at the onset of shear. Knowing that the stress is constant across the gap

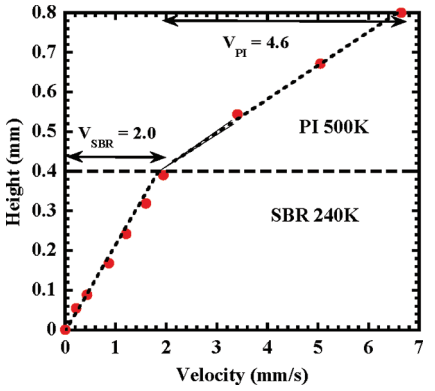

Figure 5. Velocity profile of SBR240 K/PI500 K at $\dot{\gamma} = 8.25\ s^{-1}$ from the onset of shear, $t = 0$ up to $t = 0.066$ s. The slope is related to modulus of each melt layer as shown in eq 9.

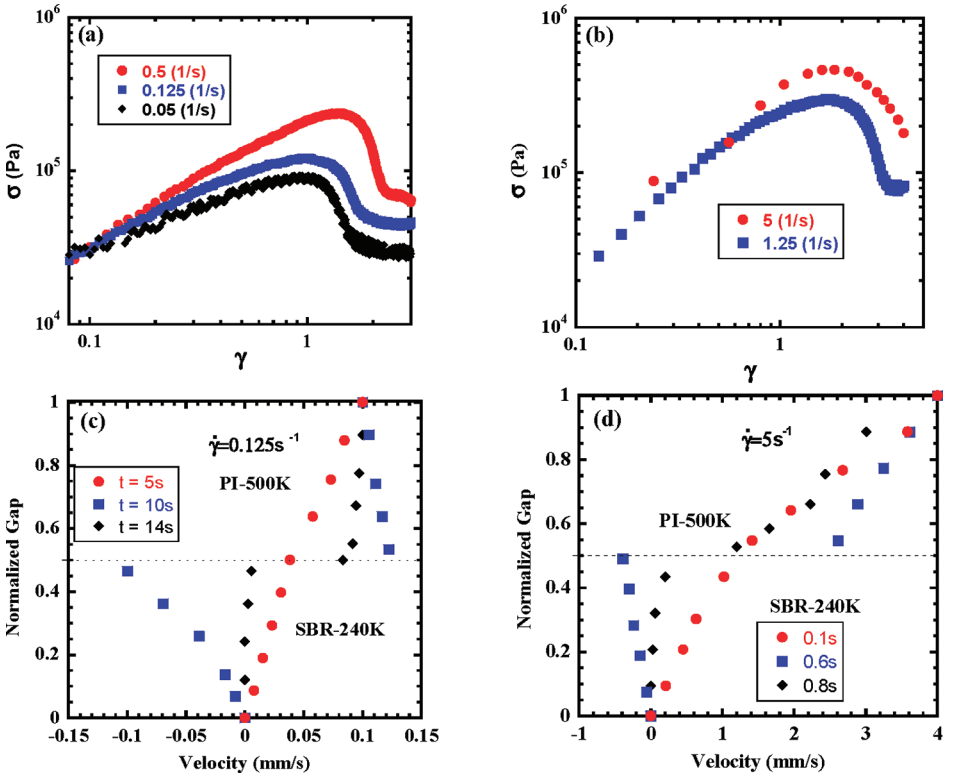

Figure 4. (a) Start up shear stress as a function of strain for the SBR/PI pair at rates less than $1\ s^{-1}$. (b) Start up shear stress as a function of strain for SBR/PI at rates greater than $1\ s^{-1}$. (c, d) Velocity profiles of SBR/PI during the startup shear whose onset is $t = 0$ for (c) $\dot{\gamma} = 0.125\ s^{-1}$ and (d) $\dot{\gamma} = 5\ s^{-1}$.

dx.doi.org/10.1021/ma201929q |*Macromolecules* 2011, 44, 9814–9820

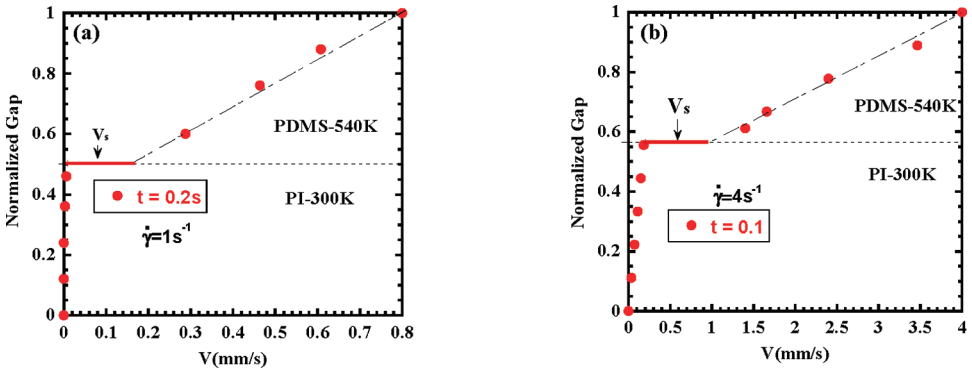

Figure 6. Velocity profiles of PDMS/PI at (a) $\dot{\gamma} = 1\ s^{-1}$ and (b) $\dot{\gamma} = 4\ s^{-1}$, where $t = 0$ s is the onset of the startup shear.

one can write the following

$$\frac{G^0_{NSBR}}{G^0_{NPI}} = \frac{\gamma_{PI}}{\gamma_{SBR}} = \frac{V_{PI}}{V_{SBR}} = 4.6/2.0 = 2.3 \qquad (9)$$

for the two layers of equal thickness. This ratio of the plateau moduli of SBR240 K to PI500 K is indeed rather close to that obtained from Table 1: $(G^0_{NSBR})/(G^0_{NPI}) = 2.05$.

In the second stage, the interface between the two layers breaks at the stress maximum. Shortly after the stress maximum, the greatest V_s is seen, this is evident at $t = 10$ s in Figure 4c and $t = 0.6$ s in Figure 4d. This increased slip velocity at the breaking point with respect to steady state is consistent with the fact that the stress is greater at the breaking point than at long times as can be seen in Figure 4a. Lastly, the sample establishes steady state as shown in Figure 4a at $t = 14$ s when Figure 4c shows the steady-state profile. There is a difference in local shear rate for PI500 K in Figures 4, parts c and d. In Figure 4d, at a higher rate and greater stress level, the PI500 K is entering a shear thinning regime according to its flow curve. But this is not the case in Figure 4c. This accounts for the large differences in local shear rates of PI500 K at $\dot{\gamma} = 0.125$ and $5\ s^{-1}$.

In contrast to the interfacial behavior of the SBR240 K and PI500 K pair, the interface between PI300 K and PDMS540 K fails at a mere shear strain of $\gamma = 0.1$ over a wide range of shear rates. This slip is apparent in Figures 6a,b. The interface between these very immiscible polymers is so weak that it could withstand little shear stress buildup.

It is useful to compare how much of the applied shear is translated into slip for the polymer pairs. Table 4 compares the ratio of V_s/V_a for the two different polymer pairs. Notice that the PDMS−PI pair have a ratio $V_s/V_a \sim 0.2$ and the SBR-PI pair have a ratio $V_s/V_a \sim 0.7$ for the rates tested. This difference arises because the PDMS melt shows less wall slip. This is due to its high entanglement molecular weight[17] $M_e \sim 10\,000$ g/mol for PDMS. As a consequence, the slip length b of eq 5 is rather small in eq 6 for V_s/V_a, leading to a smaller value for V_s/V_a. Thus, the effect of interfacial slip, measured in terms of the relative slip velocity V_s/V_a, is much smaller for the PDMS and PI pair although they are much more incompatible and have a much weaker interface. The PI/SBR interface displayed massive slip for the rates tested because each has a large b on the order of the gap size ~1 mm. These intrinsic abilities to slip allow both layers to be sheared at a considerably lower rates than the imposed apparent shear rate.

Table 4. Characteristics of Interfacial Slip Velocity

sample	V_a (mm/s)	V_s (mm/s)	V_s/V_a
PDMS-540 K/PI-290 K	1	0.17	0.17
PDMS-540 K/PI-290 K	4	0.8	0.20
SBR-240 K/PI-500 K	0.1	0.07	0.70
SBR-240 K/PI-500 K	0.04	0.027	0.68

Interfacial Yielding after Shear Cessation. We have applied PTV to observe a delayed response of the SBR240 K/PI500 K interface to step shear in a rate range of $1 \leq \dot{\gamma} \leq 12$. Specifically, the same pair studied in Figure 4, parts a−d, is step-sheared to a point before any interfacial slip is visible by PTV. Although the interface was intact during shear, we observed an interfacial breakup after shear cessation. We employed two different rates of 1.1 and $12\ s^{-1}$ respectively to shear to two strains of $\gamma = 0.6$ and 1.1 respectively. Figures 7a and 7b show the normalized stress relaxation behavior. For $\gamma = 0.6$, the stress relaxes smoothly, whereas the relaxation after shear cessation involves three stages in the case of $\gamma = 1.1$, showing a sharp dip in stage B. PTV observations reveal remarkable behavior as follows. In stage A, smooth macroscopic motions are visible, but the interface is clearly intact as seen from Figure 7c. After an induction time of 0.9s, sharp breakup is observable in stage B as shown in Figure 7c, coinciding with the steep stress decline measured in Figure 7b. In stage C, which occurs several seconds after shear cessation when the stress level drops by nearly a decade, the interface heals, and macroscopic motions are suppressed. Correspondingly, the shear stress relaxes by the mechanism of bulk chain diffusion and even exhibits a stress plateau.

When sheared to a higher strain of $\gamma \sim 1.9$, interfacial failure took place within 0.1 s after shear cessation as shown in Figure 7d. There is actually more significant slip observed in Figure 7d than in Figure 7c although the shear stress level at the onset of shear cessation is lower due to the lower applied rate of $1.1\ s^{-1}$. We note that the observed "delayed" failure, which we call arrested interfacial slip, has an identical origin to that previously reported on melt/wall arrested slip.[22] The mechanism for the arrested slip is the same as the one that produces elastic yielding in a step-strained polymer of high entanglement, i.e., the residual elastic retraction force overcoming the cohesion due to chain entanglement.[26]

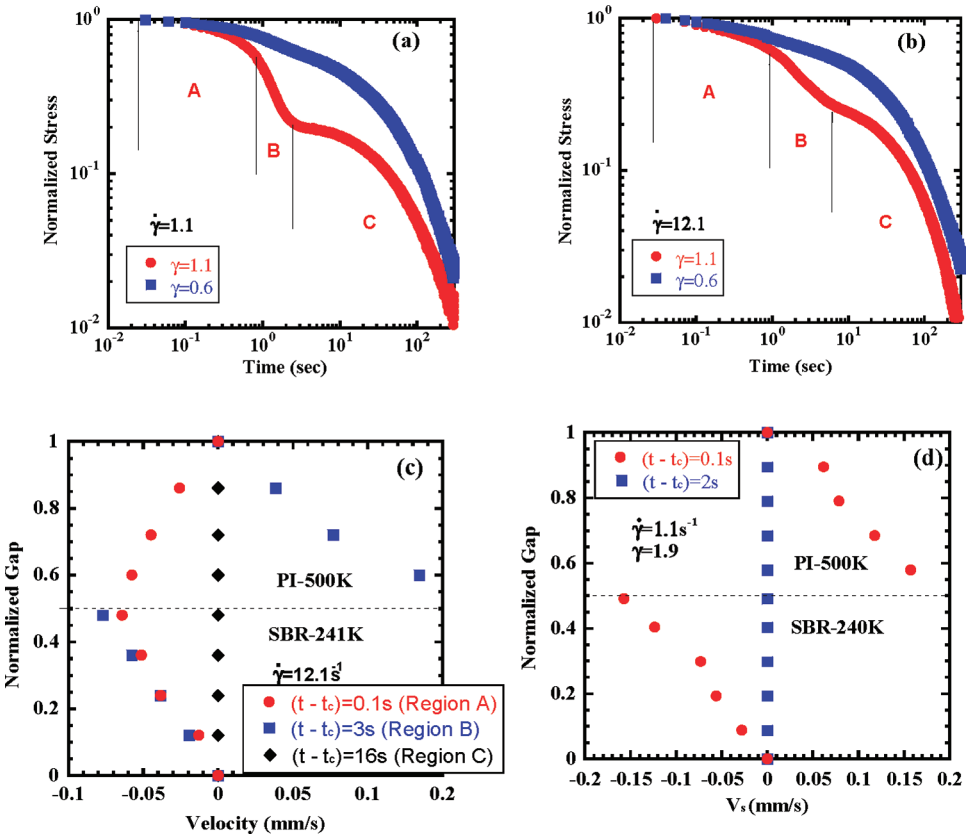

Figure 7. (a) Stress relaxation of the SBR/PI pair after step strain of $\gamma = 0.6$ and $\gamma = 1.1$ respectively applied with $\dot{\gamma} = 1.1\ s^{-1}$. (b) Stress relaxation of the SBR/PI pair after step strain of $\gamma = 0.6$ and $\gamma = 1.1$ respectively applied with $\dot{\gamma} = 12.1\ s^{-1}$. (c) PTV observations after shear cessation at $\gamma = 1.1$ applied with a rate of 12.1 s^{-1}. Here t_c is the moment of shear cessation, and $\gamma = 1.1$ is far away from the interfacial yield point around 2.0. (d) PTV observations after shear cessation at $\gamma = 1.9$ applied with a rate of 1.1 s^{-1}. Here t_c is the moment of shear cessation, and $\gamma = 1.9$ is very close to the interfacial yield point around 2.0, so that the arrested slip occurs within 0.1 s after shear cessation instead of a couple of seconds.

CONCLUSIONS

The present work follows the realization that additional insight may be gained by examining how interfacial slip is produced during startup shear. The fact that interfacial slip would not occur until after two shear strain units is rather revealing. It shows that the SBR/PI interface is quite strong, leading to the conclusion that there must be some chain entanglement between SBR and PI although they are incompatible macroscopically. Had we only examined the steady-state characteristics of this interfacial slip, we would not have obtained any information about the interfacial strength. This point highlights the purpose of the present study, which is to study the interfacial yielding using PTV observations. We conclude that there must be some level of interpenetration among the two polymers to produce considerable chain entanglement. This conclusion is consistent with the knowledge that the interfacial width is estimated to be as large as 18 nm, which is considerably larger than the entanglement spacing l_{ent} of either polymer melt listed in Table 1. The presence of sufficient chain entanglement is further hinted at by the PTV observations of arrested interfacial slip after shear cessation that involves a significant induction time. We also note the interesting macroscopic motions prior to the arrested interfacial failure. Such macroscopic motions occur because there emerges a shear stress variation across the sample gap when the two different melts start to relax their residual shear stresses at their own paces, i.e., with different relaxation times.

In contrast to the SBR/PI interface, the PDMS/PI interface is quite weak as revealed by the PTV observations. There appears to be little chain entanglement at the interface, suggesting the two melts hardly interpenetrated even at the level of entanglement spacing. The absence of entanglement between PDMS and PI is in accord with the estimated interfacial width of less than 2 nm, and the fact that both polymers entanglement length is significantly larger than this interfacial thickness. As a consequence, interfacial failure occurs before significant shear deformation takes place.

Interfacial slip between immiscible polymer pairs is an important characteristic of blends with strong chain entanglement. The degree of compatibility dictates the strength of the polymer interfaces and the slip characteristics. Conversely, by examining the critical shearing condition for interfacial yielding, we can learn about the miscibility and compatibility of polymer pairs in different light. For the example of extreme immiscibility between PDMS and PI, slip would occur within 0.1 strain units upon startup shear where the interfacial width ξ is narrower than required for chain entanglement. However due to the high M_e of PDMS, only 20% of the applied shear is taken up by the interfacial slip. In contrast, interfacial slip plays a more significant role in the pair of SBR and PI melts, absorbing 70% of the applied shear.

In summary, the strong SBR/PI interface undergoes three stages in its response to startup shear. The two-layered sample first undergoes elastic deformation where the rate of deformation

dx.doi.org/10.1021/ma201929q |*Macromolecules* 2011, 44, 9814–9820

is controlled by the respective elastic moduli of the two polymers. With increasing straining, interfacial yielding occurs as a consequence of force imbalance between the intrachain elastic retraction force and interchain gripping force.[22,27] Finally, the slip velocity attains a steady-state value at long times. Such strong interfaces also "relax" through three stages in response to a step shear of moderate magnitude. Right after shear cessation, the interface shows no sign of failure. Then an elastically driven breakup occurs at the SBR/PI interface, producing significant recoil like motions as shown in Figure 7, parts c and d. The interface heals and can sustain significant residual shear stress during the last stage of the relaxation, which occurs quiescently.

It is attempting to suggest that the characteristics reported in this study are universal. For pairs of melts with sufficient compatibility, their interfaces would be full of chain entanglement although such interfaces would still be significantly weaker than each of the bulk polymers A and B as long as A and B are not fully compatible. Conversely, highly incompatible pairs suffer interfacial failure even under rather weak shearing conditions due to lack of mutual chain penetration. However, in steady state when interfacial slip occurs, it is not the degree of compatibility but rather the degree of chain entanglement that dictates how much the interfacial slip affects the level of shear deformation that takes place in each of the individual components in the "blend".

■ ACKNOWLEDGMENT

This work is supported, in part, by a grant (DMR-0821697) from the National Science Foundation.

■ REFERENCES

(1) Brochard, F.; de Gennes, P. G. *Langmuir* **1992**, *8*, 3033.
(2) Brochard-Wyart, F.; Gay, C.; de Gennes, P. G. *Macromolecules* **1996**, *29*, 377.
(3) Ajdari, A.; Brochard-Wyart, F.; de Gennes, P. G.; Leibler, L.; Viovy, L.; Rubinstein, M. *Physica A* **1994**, *204*, 17.
(4) Drda, P. P.; Wang, S.-Q. *Phys. Rev. Lett.* **1995**, *75*, 2698.
(5) Han, C. D.; Yu, T. C. *Polym. Eng. Sci.* **1972**, *12*, 81.
(6) Lin, C. C. *Polym. J.* **1979**, *11*, 185.
(7) Utracki, L. A.; Kamal, M. R. *Polym. Eng. Sci.* **1982**, *22*, 63.
(8) Lam, Y. C.; Jiang, L.; Yue, C. Y.; Tam, K. C.; Li, L.; Hu, X. *J. Rheol.* **2003**, *47*, 795.
(9) Brown, H. R. *Annu. Rev. Mater. Sci.* **1991**, *21*, 463.
(10) Migler, K. B.; Lavallé, C.; Dillon, M. P.; Woods, S. P.; Gettinger, C. L. *J. Rheol.* **2001**, *45*, 565.
(11) Lee, P.; Park, H.; Morse, D.; Macosko, C. *J. Rheol.* **2009**, *53*, 893.
(12) Zhao, R.; Macosko., C. W. *J. Rheol.* **2002**, *46*, 145.
(13) Goveas, J. L.; Fredrickson, G. H. *Eur. Phys. J. B* **1998**, *2*, 79.
(14) Barsky, S.; Robbins, M. O. *Phys. Rev. E* **2001**, *63*, 021801.
(15) Flory, P., *Principles of Polymer Chemistry*; Cornell Univ. Press: Ithaca, NY, 1953.
(16) Helfand, E.; Tagami, Y. *Polym. Lett.* **1971**, *9*, 741.
(17) De Gennes, P. G. *C. R. Acad. Sci.* **1979**, *288B*, 219.
(18) Zhao, R.; Macosko., C. W. *J. Rheol.* **2002**, *46*, 145.
(19) Fetters, L. J.; et al. *Macromolecules* **1994**, *27*, 4639.
(20) Eitouni, H.; Balsara, N. Thermodynamics of Polymer Blends. In *Physical Properties of Polymer Handbook*, 2nd ed.; Mark, J. E., Ed.; 2006; 339.
(21) Estimate for infinite degree of polymerization used since $N >$ 1000 in all polymers.
(22) Wang, S. Q. *Macromol. Mater. Eng. Sci.* **2007**, *129*, 215.
(23) Boukany, P. E.; Wang, S. Q. *J. Rheol.* **2007**, *51*, 217.
(24) Boukany, P. E.; Wang, S. Q. *Macromolecules* **2009**, *42*, 2222.
(25) Boukany, P. E.; Wang, S. Q.; Wang, X. R. *Macromolecules* **2009**, *42*, 6261.
(26) Wang, S. Q.; Ravindranath, S.; Wang, Y.; Boukany, P. *J. Chem. Phys.* **2007**, *127*, 064903.
(27) Wang, Y. Y.; Wang, S. Q. *J. Rheol.* **2009**, *53*, 1389.